Diagnosing the Conditional Probability of Tornado Damage Rating Using Environmental and Radar Attributes

BRYAN T. SMITH, RICHARD L. THOMPSON, ANDREW R. DEAN, AND PATRICK T. MARSH

NOAA/NWS/NCEP/Storm Prediction Center, Norman, Oklahoma

(Manuscript received 2 October 2014, in final form 22 April 2015)

ABSTRACT

Radar-identified convective modes, peak low-level rotational velocities, and near-storm environmental data were assigned to a sample of tornadoes reported in the contiguous United States during 2009–13. The tornado segment data were filtered by the maximum enhanced Fujita (EF)-scale tornado event per hour using a 40-km horizontal grid. Convective mode was assigned to each tornado event by examining full volumetric Weather Surveillance Radar-1988 Doppler data at the beginning time of each event, and 0.5° peak rotational velocity (V_{rot}) data were identified manually during the life span of each tornado event. Environmental information accompanied each grid-hour event, consisting primarily of supercell-related convective parameters from the hourly objective mesoscale analyses calculated and archived at the Storm Prediction Center. Results from examining environmental and radar attributes, featuring the significant tornado parameter (STP) and 0.5° peak V_{rot} data, suggest an increasing conditional probability for greater EF-scale damage as both STP and 0.5° peak V_{rot} increase, especially with supercells. Possible applications of these findings include using the conditional probability of tornado intensity as a real-time situational awareness tool.

1. Introduction

Considerable effort in recent decades has focused on near-storm environment interrogation via observed soundings (e.g., Rasmussen and Blanchard 1998; Rasmussen 2003; Craven and Brooks 2004), model-based planar fields (e.g., Stensrud et al. 1997), and model-based proximity soundings in order to discriminate between nontornadic and significant [rated as category 2 or greater on the Fujita scale (≥F2)] tornado environments for supercells (e.g., Thompson et al. 2003, 2007; Davies 2004; Davies and Fischer 2009). These investigations provided empirical evidence supporting the importance of several measures of moisture, buoyancy, and vertical wind shear for producing significant tornadoes with supercells, as reflected in the development of supercell ingredients–based composite parameters [e.g., significant tornado parameter (STP[1]); Thompson et al. (2003)]. Convective mode is an additional component widely recognized as a contributor to the occurrence and nonoccurrence of severe weather. Recent work by Smith et al. (2012, hereafter S12) demonstrated relationships of convective mode and storm-scale rotation (when applicable) to tornado damage intensity, and the second part of that study, by Thompson et al. (2012, hereafter T12), went a step further and investigated the relationships between the near-storm environment and these storm attributes.

The infusion of real-time diagnostic parameters, like the National Oceanic and Atmospheric Administration/National Weather Service/Storm Prediction Center's (NOAA/NWS/SPC) hourly mesoanalysis (Bothwell et al. 2002), can contribute to greater awareness of potential tornado risk in an operational forecast and warning setting. Magsig (2008) discussed techniques for diagnosing radar-based storm attributes and integrating environmental information into the warning decision-making process. Recent work by Brotzge et al. (2013) revealed NWS tornado warning performance, as measured by probability of detection, was maximized for the more intense tornado events [i.e., higher enhanced Fujita (EF)-scale damage ratings] when the tornadoes were produced by discrete supercells with strong mesocyclones, close to the radar site, and in

[1] STP effective-layer calculation (T12) only discussed herein, for the nearest hour preceding each event.

Corresponding author address: Bryan T. Smith, NOAA/NWS/NCEP/Storm Prediction Center, 120 David L. Boren Blvd., Ste. 2300, Norman, OK 73072.
E-mail: bryan.smith@noaa.gov

DOI: 10.1175/WAF-D-14-00122.1

environments strongly supportive of tornadic supercells. Real-time utilization of the multicomponent datasets described in T12 and Brotzge et al. (2013) may contribute to the improved situational awareness of tornado potential.

In light of recent tornado disasters (e.g., 27 April and 22 May 2011, among others), contemporary efforts within the NWS, as part of the Weather Ready Nation initiative, have sought to better assess tornado vulnerability and better communicate impact-based hazard information (i.e., tornado risk) to the public. One such example involves NWS Central Region local forecast offices tasked with issuing experimental impact-based warnings (IBWs; Wagenmaker et al. 2014) for severe thunderstorms and tornadoes. IBWs are intended to convey the potential impact to life and property within the disseminated warning text based on the predicted intensity of the severe hazard (e.g., tornado). Future warn-on-forecast (Stensrud et al. 2009) work will likely include explicit probabilistic information in addition to the binary tornado warning decision point in current use.

Developmental work from recent studies (e.g., Kingfield et al. 2012; LaDue et al. 2012) examined the relationship between storm-scale circulation algorithms using Weather Surveillance Radar-1988 Doppler (WSR-88D) and EF-scale damage ratings in a diagnostic manner. A manual user-defined maximum low-level velocity difference (LLVD) was found by LaDue et al. (2012) to exhibit a stronger linear relationship to EF-scale rating on a small number of high-resolution tornado damage surveys compared to an automated LLVD approach using either the mesocyclone detection algorithm (MDA; Stumpf et al. 1998) or the tornado detection algorithm (TDA; Mitchell et al. 1998). Newman et al. (2013) found utility in applying range correction to the local, linear least squares derivatives (LLSDs; Smith and Elmore 2004) azimuthal shear algorithm, and this procedure aided in differentiating between nontornadic and tornadic radar scans for a small number of events. Blair and Leighton (2014) noted the need for robust, scientific guidance for real-time tornado intensity estimates in their assessment of event confirmation in NWS warnings and statements across the central continental United States (CONUS) from 2007 to 2011. The early studies investigating the relationship between tornado intensity and radar (e.g., Kingfield et al. 2012; LaDue et al. 2012; Toth et al. 2013) have shown some ability to identify different levels of tornado intensity in a diagnostic manner, thereby lending credence to the underlying idea of tornado intensity identification, from which IBW is based.

Though forecasts of tornado intensity, on the spatiotemporal scales of tornado warnings, remain a daunting task, this study strives to construct a tornado database that can provide diagnostic information on tornado intensity (as inferred by EF-scale damage ratings), given that a tornado has developed (i.e., conditional probability). This study builds upon previous work by S12 and T12 by further developing a multicomponent dataset, which includes 0.5° peak rotational velocity (V_{rot}) information, rather than mesocyclone nomograms (Andra 1997; Stumpf et al. 1998), to assess storm-scale rotation strength. In addition, other classifiable circulations [e.g., mesovortex; Trapp and Weisman (2003)] and their strengths were also examined. This study advocates combining near-storm environment information and a relatively simple, real-time radar diagnosis to better assess the maximum conditional tornado intensity risk—a necessary step in improving both the consistency of tornado warnings and near-term forecasts of tornado intensity.

2. Data and methodology

a. Data and event filtering

Radar-identified convective modes, peak low-level rotational velocities, and near-storm environmental data were assigned to a sample of tornadoes reported in the CONUS during the 2009–13 period, which corresponds with most of the WSR-88D superresolution data era (Torres and Curtis 2007). The tornado segment data were filtered by the maximum EF-scale tornado damage rating per hour on a 40-km horizontal grid, and after additional filtering described herein (section 2c), yielded a total of 4770 tornado grid-hour events (hereafter tornado events). Convective mode was assigned to each tornado event via manual examination of full volumetric WSR-88D data (section 2b) at the beginning time of each event, and 0.5° peak V_{rot} was determined manually using superresolution radar data during the life span of each tornado event (section 2c). Environmental information, consisting primarily of supercell-related convective parameters from the hourly SPC objective analyses, accompanied each tornado event.

Within the framework described above, the authors made careful manual adjustments to a small portion (7.9%) of the database. Many of the suspected report errors involved incorrectly listed report times, as determined by time matching the reports to radar data. Examples of this suspected error type included reports well removed from existing radar echoes and time displaced on the order of tens of minutes to an hour or more. In situations where a suspected error could not be

corrected easily, the NCDC publication *Storm Data* was used to examine the description of the questionable reports in an effort to identify the storm responsible for the event. Despite alleviating most errors, small time discrepancies on the order of one or two volume scans (51% of all events exhibiting error had time displacement errors ≤10 min) were found in *Storm Data* between the beginning time of a tornado event and pertinent WSR-88D velocity signatures, similar to a finding by French et al. (2013) using a mobile radar. Unless a time or location change was necessary based on a well-resolved circulation, we deferred to the NWS-documented begin time and location, in an attempt to account for uncertainty and variability in distance between the tornado location relative to the WSR-88D circulation location (e.g., Speheger and Smith 2006).

b. Radar-based storm mode classification criteria

The Gibson Ridge Level II Analyst radar-viewing software (http://www.grlevelx.com/) was used to analyze archived WSR-88D level-II single-site radar data (Crum et al. 1993) from the National Climatic Data Center (http://www.ncdc.noaa.gov/nexradinv/) using the closest radar (within 101 mi) to classify convective mode based on S12. Convective mode was determined using full volumetric radar data, especially when data through a deep layer were needed to perform a more thorough assessment of storm structure. Convective mode was assigned based on the volume scan and lower-elevation tilts (e.g., 0.5°) of base reflectivity immediately prior to the time of the tornado event. Emphasis herein is placed on the three major convective mode classes of tornadic storms: supercells[2] (3392 events), quasi-linear convective systems (QLCSs; 894 events), and disorganized cells/clusters and marginal supercells (484 events; hereafter referred to as other modes).

Discrete or embedded cells with focused areas of cyclonic (or anticyclonic) azimuthal shear were further scrutinized as potential supercells, following the mesocyclone nomograms developed using 4-bit radar data [after Andra (1997) and Stumpf et al. (1998)]. Supercells required a peak rotational velocity $\geq 10\,\mathrm{m\,s^{-1}}$ (i.e., a peak-to-peak azimuthal velocity difference of roughly $20\,\mathrm{m\,s^{-1}}$ over a distance of less than ~7 km), rotation ≥ ¼ the depth of the storm, and rotation duration of at least 10–15 min. Circulations were classified as weak shear (nonsupercell), and weak, moderate, or strong supercells, following the range-dependent horizontal peak rotational velocity values for the 1-, 2-, and 3.5-nautical mile (n mi; 1 n mi = 1.852 km) mesocyclone nomograms. Storms that exhibited persistent, weak azimuthal shear just below the nomogram's minimal mesocyclone threshold and transient supercell reflectivity structure, or identifiable rotation (regardless of magnitude) for no more than two consecutive volume scans (i.e., <10 min), were binned in the marginal supercell (i.e., other) category.

A QLCS is defined as consisting of contiguous reflectivity at or above the threshold of 35 dBZ for a horizontal distance of at least 100 km and a length-to-width aspect ratio of at least 3:1 at the time of the event, similar to Trapp et al. (2005). Other modes included disorganized cellular modes that did not include supercell structures (e.g., single cell, multicell) and consisted mainly of conglomerates meeting the reflectivity threshold but not satisfying either supercell or QLCS criteria (e.g., short line segment). Additionally, storms exhibiting transient (i.e., one or two volume scans) rotation below supercell rotation criteria were assigned to the other modes category. For a more thorough discussion pertaining to the complexity and challenges of categorizing convective mode, please refer to S12.

c. Low-level rotational velocities

Peak inbound and outbound velocities were examined for each volume scan from immediately prior to tornado formation through tornado dissipation. Only combinations of velocity maxima exhibiting cyclonic or anticyclonic azimuthal shear within 5 n mi and ≤45° angle from one another were considered, to avoid primarily convergent or divergent signatures. The maximum peak rotational velocity [$V_{rot} = (|V_{in}| + |V_{out}|)/2$], from all volume scans was assigned to each tornadic event (Fig. 1), and only tornado events sampled at or below 10 000 ft (i.e., ≤101-mi range) height above radar level (ARL) were analyzed and included in this study (Fig. 2).

Although the peak V_{rot} only uses a pair of data points that can be influenced by errors due to aliasing or "noisy data" (Wood and Brown 1997), this dataset considers multiple possible pairs of peak velocity data for individual volume scans during the tornado's lifetime. This approach can effectively reduce the influence of any volume scan(s) with potential data errors by defaulting to other candidate volume scans. Concerns such as radar beam placement relative to the tornado circulation were partially mitigated by the large sample size of tornado events and by two or more volume scans per tornado event. Underestimates of 0.5° peak V_{rot} owing to beam offset would likely be applied randomly throughout the dataset. Ancillary data such as the time of the volume scan and a subjective binary assessment of a clear/tight circulation were also found for the majority of tornado

[2] Includes right-moving supercells (3384) and left-moving supercells (8).

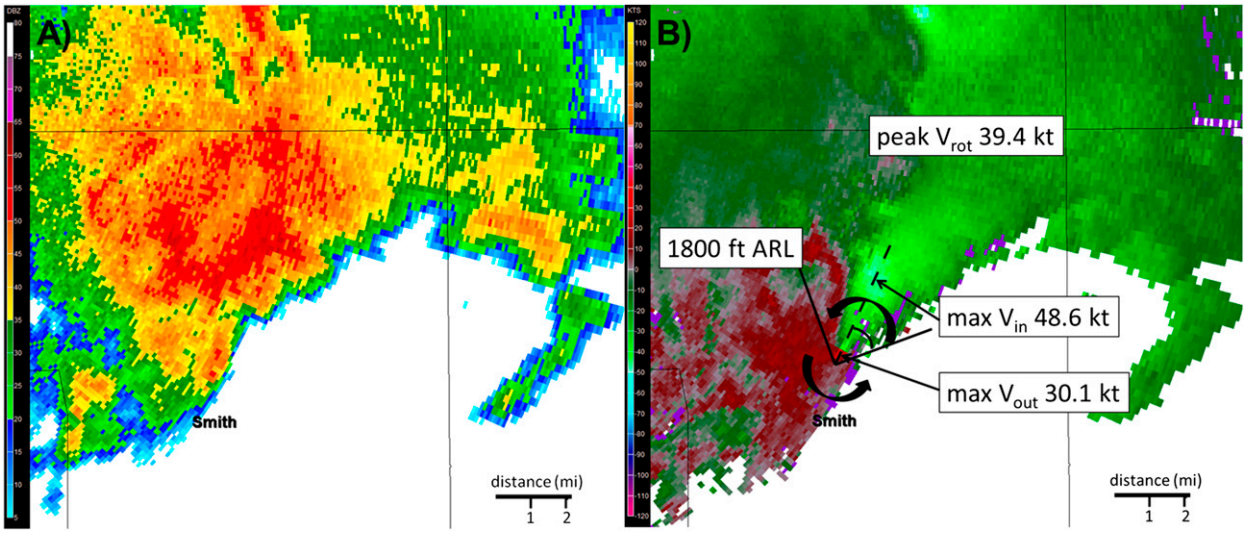

FIG. 1. (a) WSR-88D base reflectivity (dBZ; color scale on left) at 0.5° beam tilt from Jackson, MS (KDGX), at 0852 UTC 30 Nov 2010. A cell-in-cluster supercell produced an EF2 tornado in Smith County, MS (start time 0844 UTC). North is up, county borders are black, and distance scale is at lower right. (b) As in (a), but for storm-relative velocity (kt; color scale on left), 45° angle insert, and curved arrows signifying rotation. Denoted inserts display maximum inbound storm-relative velocity (max V_{in}, 48.6 kt), maximum outbound storm-relative velocity (max V_{out}, 30.1 kt), 0.5° peak V_{rot} (39.4 kt), and velocity sampled height ARL (1800 ft).

events (3690 of 4770). Finally, the sampling of circulations by ARL (nearest 100 ft) using the highest radar bin between the two peak V_{rot} data points was documented in order to account for the effects of radar beam widening with range that reduce the ability of the WSR-88D to resolve storm-scale circulations. Unlike Toth et al. (2013) and LaDue et al. (2012), velocity data were not dealiased manually beyond the existing dealiasing algorithm capability for several reasons: 1) our peak V_{rot} method is easily reproduced in real-time forecast and

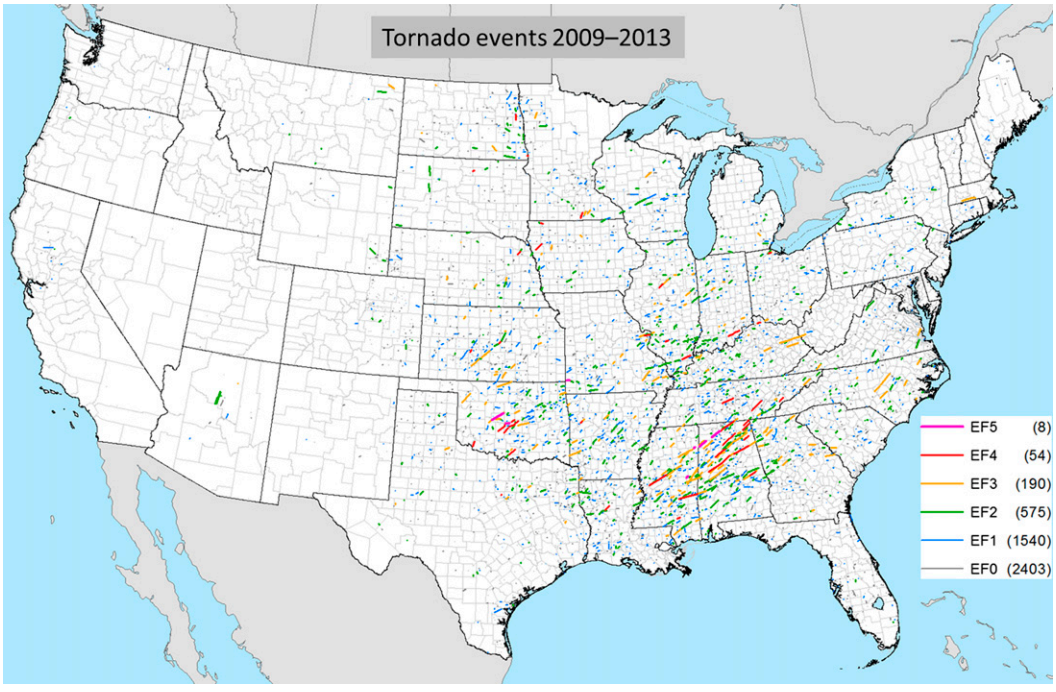

FIG. 2. Spatial plot of tornado events sampled at ≤10 000 ft ARL.

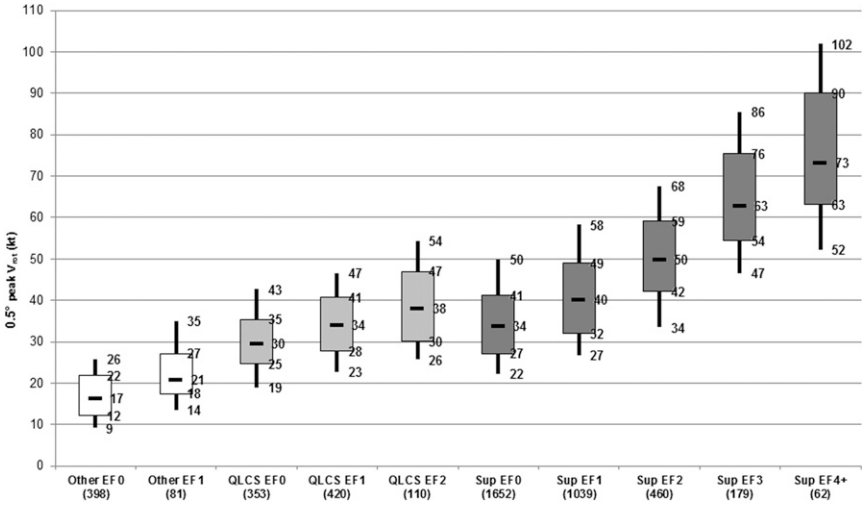

FIG. 3. Box-and-whiskers plot of 0.5° peak V_{rot} (kt) of EF0–EF5 tornado events (2009–13; at ≤10 000 ft ARL, with 1–101-mi radius) grouped by supercell (Sup; dark gray), QLCS (light gray; EF3 events not shown), and other modes (Other; white). The shaded boxes span the 25th–75th percentiles, and the whiskers extend upward to the 90th and downward to the 10th percentiles. Median values are marked within the box, and sample sizes for each storm mode and EF-scale category are shown in parentheses.

warning operations with short time constraints and 2) the impact of not dealiasing a small fraction of tornado velocity signatures is likely minimized by the large size of this sample (4770 tornado events). The velocity dealiasing algorithm technique used by Gibson Ridge Analyst software is similar to current and legacy dealiasing techniques for WSR-88D data (e.g., Eilts and Smith 1990; Zittel and Jing 2012).

Although tornado circulations appeared to be resolved explicitly in a few cases with large tornadoes close to the radar site, an overwhelming majority of WSR-88D velocity signatures were representative of the larger tornadic vortex (Mitchell et al. 1998) or the low-level mesocyclone (Stumpf et al. 1998). A relatively small percentage of available cases (11%) consisted of 0.5° peak V_{rot} diameters exceeding 3.5 mi, which is clearly

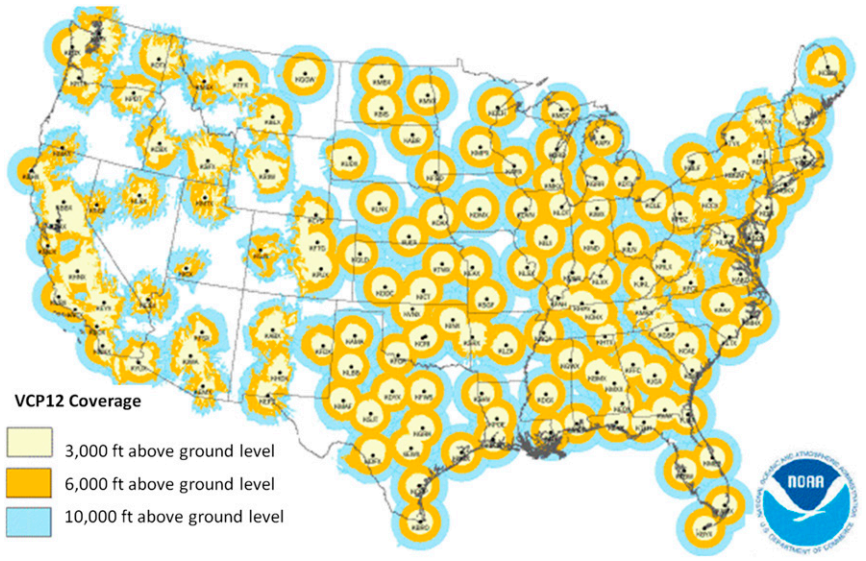

FIG. 4. NEXRAD coverage at or above 3000, 6000, and 10 000 ft or less AGL (ROC 2014). The level refers to the center of the beam height (assuming standard atmospheric refraction). Terrain blockage indicated where 50% or more of the beam is blocked.

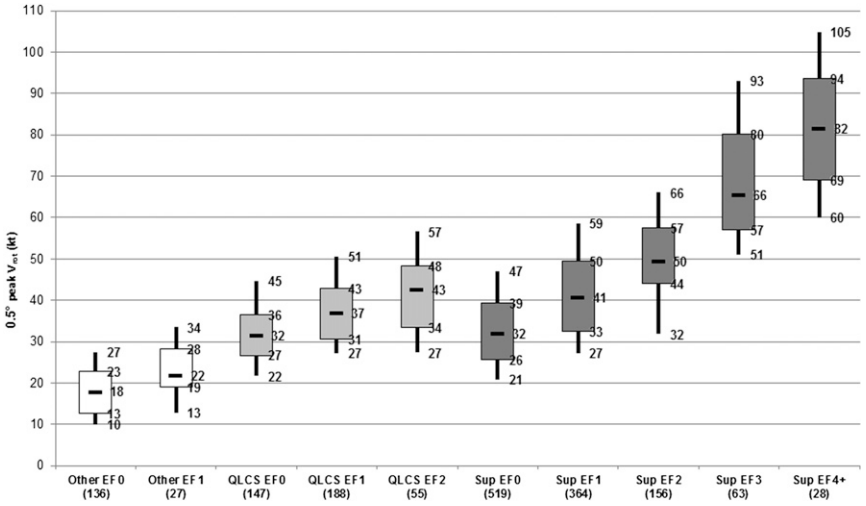

FIG. 5. As in Fig. 3, but for tornado events at 100–2900 ft ARL, with 1–42-mi radius.

larger than any documented tornado diameter. While many 0.5° peak V_{rot} cases were easily assessed, 0.5° peak V_{rot} identification at times was a challenging task and involved considerable effort and uncertainty in assigning the peak inbound and peak outbound values. A neighborhood approach was effectively used on a small subset of events (~3.6%) because of increased uncertainty in assigning the 0.5° peak V_{rot}. Apparent bad radials in velocity data were not used and other nearby velocity bins were used instead. Other questionable velocity signatures included noisy data, which clearly suffered from dealiasing problems. These difficult-to-assign cases were in most situations assigned peak inbound and outbound velocity values nearby. Less often, the rotational velocity from the next highest volume scan was recorded. A 5–10-knot (kt; 1 kt = 0.51 m s^{-1}) difference in 0.5° peak V_{rot} was typical between seemingly erroneous V_{rot} and the V_{rot} recorded, and resulted in a reduced value than otherwise would have been assigned. If a tight circulation couplet (i.e., likely resolving the tornado vortex) was clearly separate from other nearby higher-velocity bins, the velocity data associated with the smaller-scale circulation were preferentially recorded; otherwise, preference was given to recording velocity information within the larger-scale circulation if the outer circulation V_{rot} value was more than 5 kt greater than the candidate V_{rot} value of the inner circulation.

The manual analysis of velocity data presented here is similar to techniques used in real-time warning

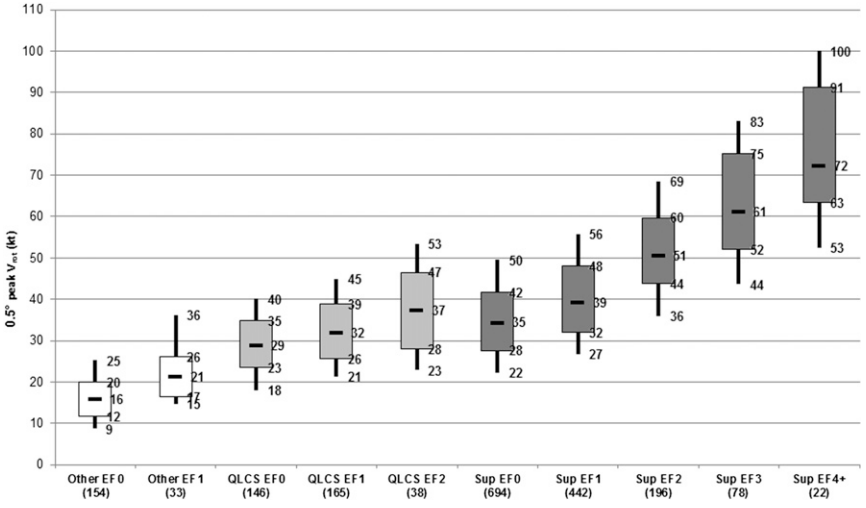

FIG. 6. As in Fig. 3, but for tornado events at 3000–5900 ft ARL, with 42–70-mi radius.

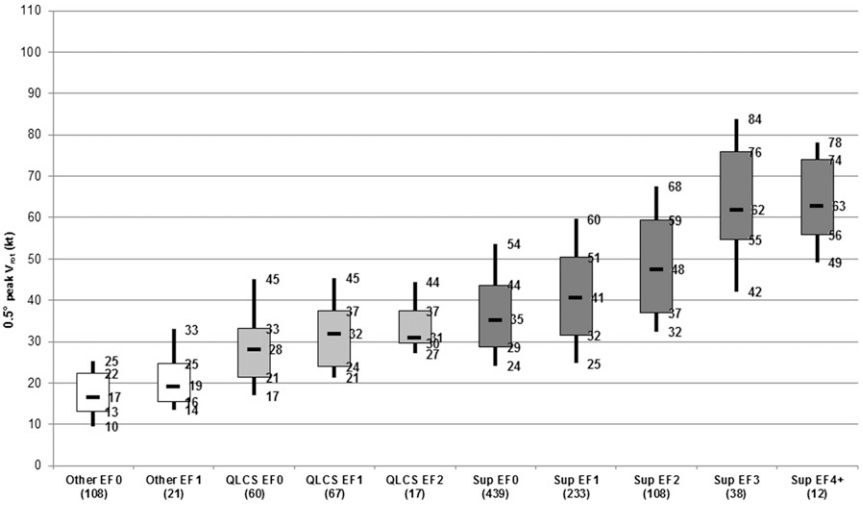

FIG. 7. As in Fig. 3, but for tornado events at 6000–10 000 ft ARL, with 70–101-mi radius.

decision-making. The subjective analysis used to diagnose circulation strength can be advantageous compared to an automated objective approach, especially in cases when radar algorithms do not resolve some tornadic circulations [e.g., landspouts; Brady and Szoke (1989)] because of resolution limitations, or when circulations are misidentified along squall lines aligned along the radar beam.

While it was common for velocity signatures to vary during the life cycle of the tornado event, the tornado events in this sample rarely had one outlier volume scan at 0.5° tilt with much stronger V_{rot} compared to the other sampled volume scans. Many of the higher-end tornado cases exhibited consistent velocity values that were just below the peak V_{rot} value at least for several volume scans, including a substantial part of the tornado segment grid hour (i.e., tornado event). Although there was a strong correspondence between the highest EF-scale rating and the maximum 0.5° peak V_{rot}, the two did not necessarily match in time and space.

d. *Quality of SPC hourly mesoscale analyses*

Rapid Update Cycle (RUC; Benjamin et al. 2004) model 0- and 1-h forecasts provided the basis for the SPC hourly mesoscale analyses from January 2003 through April 2012. Coniglio (2012) evaluated the SPC hourly objective analyses via VORTEX2 field project soundings from the springs of 2009 and 2010 across the Great Plains and found that the SPC analyses improved upon the background 1-h RUC model forecasts of surface temperature and dewpoint temperature, as well as many derived thermodynamic variables. However, errors were still substantial on occasion (especially above the ground) and large enough to be of concern regarding expected storm evolution. The RUC model was replaced by the Rapid Refresh (RAP) model in May 2012, though comparisons of the RUC and RAP in severe storm environments are lacking in the formal literature. Laflin (2013) examined vertical profiles of temperature and moisture for rawinsonde observations and RAP model soundings and quantified differences in terms of buoyancy [e.g., lowest 100-hPa mean-layer convective available potential energy (MLCAPE)] with a convective-related focus on the preconvective boundary layer. Substantial errors were found in RAP 6- and 12-h forecasts of boundary layer moisture, which resulted in underestimates of buoyancy (e.g., surface-based CAPE errors approaching 1000 J kg^{-1}) in dry, well-mixed environments. Yet Laflin (2013) covered only a limited domain (six Great Plains rawinsonde sites) during 7 weeks in the late spring 2012, and the findings may not be representative of 0- and 1-h RAP soundings used in the SPC objective analyses, or of other environments supportive of tornadoes (e.g., Thompson et al. 2013).

Mesoscale observations, such as trends in WSR-88D vertical wind profile data, may aid situational awareness, especially for cases when background objective hourly guidance differs substantially from the strength of radar-derived wind fields (Guyer and Hart 2012). Potvin et al. (2010) discussed proximity sounding sensitivity to spatiotemporal distance from an event. When examining 0–1-h proximity sounding data, Potvin et al. (2010) identified a zone within 40–80 km of the launch site (see their Fig. 5) that served to best characterize the near-storm environment (e.g.,

TABLE 1. Mean (median) values of 0.5° peak V_{rot} and STP_{80km} for supercell (Sup) and QLCS tornado events by EF-scale class.

	Sup EF0	Sup EF1	Sup EF2	Sup EF3	Sup EF4+	QLCS EF0	QLCS EF1	QLCS EF2
V_{rot}	35 (34)	41 (40)	51 (50)	65 (63)	76 (73)	30 (30)	35 (34)	39 (38)
STP_{80km}	2.7 (1.9)	3.3 (2.6)	4.0 (3.4)	5.5 (4.6)	8.4 (8.4)	1.6 (1.0)	2.1 (1.7)	2.6 (2.2)

minimize convective feedback effects, maintain close distance). The findings of Potvin et al. (2010) were reinforced by Parker (2014), who examined the spatiotemporal variability of VORTEX2 field project soundings relative to both tornadic and nontornadic supercells. Parker (2014) noted that pronounced differences in environmental characteristics extended beyond the storm-induced inflow region, with more favorable combinations of low-level moisture and vertical wind shear evident well away from a small sample of tornadic supercells compared to nontornadic supercells. Still, variability in the near-storm environment was substantial, and a single proximity sounding is not necessarily reflective of supercell tornado potential.

This study utilized the maximum neighborhood grid-hour value within 80 km of each tornado event for STP (hereafter STP_{80km}; T12) to account for proximity concerns and the spatial variability of environmental parameters while providing a relatively simple characterization of the tornado environments that were dominated by supercells. The maximum neighborhood approach reflects the ability of the operational meteorologist to consider more than a single gridpoint value, and to alleviate potential spatial errors in the model-based parameter fields. An example of using the neighborhood grid-hour value versus the grid-hour value is demonstrated by the Rozel, Kansas, EF4 tornado on 18 May 2013: STP_{80km} reached 4.5 compared to the 40-km grid-hour value of 0.0 in a case with a tornadic storm in proximity to sharp gradients of low-level moisture and buoyancy.

e. Conditional tornado probabilities

Conditional (i.e., upon the occurrence of a tornado) probabilities of tornado intensity, as measured by EF-scale damage, are calculated using STP_{80km} and 0.5° peak V_{rot}. Given the large range in documented STP_{80km} (0–24), 0.5° peak V_{rot} (0–124 kt), and EF scale (0–5), the sample sizes for paired values of STP_{80km} to EF scale and 0.5° peak V_{rot} to EF scale are severely limited in most cases. Therefore, each STP_{80km} value was placed within a bin (e.g., 4.00–5.99), and each 0.5° peak V_{rot} value below 100 kt was placed within a 10-kt bin (e.g., 60.0–69.9 kt).

3. Results

a. 0.5° peak V_{rot}

A strong relationship exists between 0.5° peak V_{rot} and EF scale for all convective modes. For higher EF-scale ratings, an increase in the 0.5° peak V_{rot} distribution occurred (Fig. 3). Prior studies (e.g., Wood and Brown 1997; Newman et al. 2013) have documented the dependence of decreased circulation resolution as a function of increased radar range (and height ARL). Therefore, 0.5° peak V_{rot} data used to sample tornado events were rounded to the nearest 100 ft ARL and separated into three ARL (radar range) groups: 100–2900, 3000–5900, and 6000–10 000 ft (Fig. 4). A largely monotonic increase for 0.5° peak V_{rot} is displayed for tornado events as the supercell EF scale increases for events sampled below 6000 ft ARL (Figs. 5 and 6), or within 70 mi of the radar site.[3] For events sampled at 6000–10 000 ft ARL (Fig. 7), little difference in the distribution is evident among EF3 and EF4 supercells or greater (hereafter EF4+) events. Comparing the supercell EF4+ events among the three radar ARL groups (Figs. 5–7) shows a decrease in 0.5° peak V_{rot} magnitudes at the 10th, 25th, 50th, 75th, and 90th percentiles as ARL height (range) increases, particularly between the 100–2900 and 6000–10 000 ft ARL groups. This suggests that radar sampling of velocities is limited as horizontal distance from the radar increases, through broader beamwidth and corresponding lower horizontal resolution (Wood and Brown 1997). In other words, the WSR-88D more clearly resolves the stronger and smaller-diameter circulations with EF4+ tornado events closer to the radar, while radar sampling primarily reflects the mesocyclone at greater distances (elevations). Some caution is warranted in the interpretation of the EF4+ tornado events in Fig. 7, given a sample size of only 12 cases.

Comparisons of 0.5° peak V_{rot} and storm mode were also completed. One possible contributor to the mismatch between 0.5° peak V_{rot} and storm mode for similar EF-scale damage rating (cf. Figs. 3 and 5–7) is the inability of the WSR-88D to resolve the generally

[3] See Fig. 4 for an approximation of the areal coverage of the WSR-88D radar below 3000 and 6000 ft ARL (ROC 2014).

TABLE 2. Mean differences in 0.5° peak V_{rot} and STP_{80km} for supercells (Sup). Parameter units are the same. Boldface differences are statistically significant at $\alpha < 0.001$, and boldface and italic differences are considered to be sufficiently large to be of operational significance (i.e., $V_{rot} > 20$, STP > 4).

	Sup EF4+ − Sup EF0	Sup EF4+ − Sup EF1	Sup EF4+ − Sup EF2	Sup EF4+ − Sup EF3	Sup EF3 − Sup EF0	Sup EF3 − Sup EF1	Sup EF3 − Sup EF2
V_{rot}	***41***	***35***	***26***	**12**	***30***	***23***	**14**
STP80km	***5.8***	***5.1***	***4.4***	**2.9**	***2.8***	**2.2**	**1.5**

shallower vertical depths and smaller horizontal dimensions of the QLCS and other modes of tornadic storm circulations compared to their larger supercell counterparts. However, miniature supercells (e.g., Davies 1993) and their smaller-scale mesocyclone circulations on radar (e.g., Kennedy et al. 1993; Burgess et al. 1995; Grant and Prentice 1996)—often found in low-CAPE and high-shear environments (e.g., Davis and Parker 2014)—can also pose a challenge in identifying rotation due partially to shallower and smaller-diameter circulations.

b. *Convective mode and 0.5° peak V_{rot}*

S12 found that variations in tornado EF-scale damage ratings were more closely related to mesocyclone strength than the specific type of right-moving supercell (discrete cell, cell in cluster, or cell in line). Based on the findings of S12, weak mesocyclones were most common with weak tornadoes (EF0 and EF1), whereas strong mesocyclones were almost exclusively associated with EF3+ tornadoes when examining the volume scan prior to the tornado start time. This study revealed a general increase in 0.5° peak V_{rot} as EF scale increased for all three convective modes (i.e., supercell, QLCS, and other modes; Figs. 3 and 5–7). Around one quartile difference in 0.5° peak V_{rot} was found when compared to ±1 supercell EF-scale rating class (Fig. 3). Mean 0.5° peak V_{rot} values increased for each supercell EF-scale rating class increase (Table 1). Differences in mean 0.5° peak V_{rot} values for EF4+ versus EF0, EF4+ versus EF2, and EF2 versus EF0 were 41, 26, and 15 kt, respectively (Tables 2 and 3). All differences in EF-scale rating classes among supercells (Tables 2 and 3) were statistically significant at $\alpha < 0.001$ for a two-tailed Student's *t* test with unequal variances (Wilks 2006). A quartile difference ≥1 is evident between QLCS EF0 and EF2 events and was also statistically significant at $\alpha < 0.001$ for a two-tailed Student's *t* test (Table 3). While differences in mean 0.5° peak V_{rot} values comparing lower EF-scale-rated supercell and QLCS were deemed statistically significant, these differences are of little practical significance in operations (Tables 3 and 4). Tornado events from QLCS and other modes possessed substantially weaker 0.5° peak V_{rot} than supercells (Figs. 3 and 5–7). Storms in the other modes category were disproportionately more difficult to assign 0.5° peak V_{rot} because of their weaker and more ambiguous rotational signatures.

Supercell tornado events were rated roughly one EF-scale category less than QLCS tornado events with similar 0.5° peak V_{rot} distributions (Fig. 3; cf. the QLCS EF1 distribution to supercell EF0). Hence, QLCS and other modes tend to be associated with weaker 0.5° peak V_{rot} values than supercells that produce similar damage. In addition, the majority of QLCS tornadoes in our sample were reported near and east of the Mississippi River (S12), where tornado damage paths may be revealed more consistently by greater population and vegetation densities compared to the Great Plains. This assertion is supported by mobile radar observations collected primarily in the Great Plains (Alexander and Wurman 2008).

c. *Near-storm environment*

Based on past studies (e.g., Thompson et al. 2003; T12), STP exhibited greater skill in discriminating between nontornadic and significantly tornadic supercell environments compared to any of its individual components or any other parameters among the 38-variable database at the SPC (see Table A1 in the appendix). The near-storm environment portion of this study focuses on the STP and provides two examples of associating STP with a tornado event. Using either the nearest STP

TABLE 3. As in Table 2, but for Sup − Sup, QLCS − QLCS, and Sup − QLCS differences.

	Sup EF2 − Sup EF0	Sup EF2 − Sup EF1	Sup EF1 − Sup EF0	QLCS EF2 − QLCS EF1	QLCS EF2 − QLCS EF0	QLCS EF1 − QLCS EF0	Sup EF2 − QLCS EF2	Sup EF2 − QLCS EF1
V_{rot}	**15**	**9**	**6**	**4**	**9**	**4**	**11**	**16**
STP_{80km}	**1.3**	**0.7**	**0.7**	0.5	**1.0**	**0.5**	**1.5**	**2.0**

TABLE 4. As in Table 3, but for Sup − QLCS differences.

	Sup EF2 − QLCS EF0	Sup EF1 − QLCS EF2	Sup EF1 − QLCS EF1	Sup EF1 − QLCS EF0	Sup EF0 − QLCS EF2	Sup EF0 − QLCS EF1	Sup EF0 − QLCS EF0
V_{rot}	**20**	2	**7**	**11**	**4**	0	**5**
STP_{80km}	**2.4**	**0.8**	**1.3**	**1.8**	0.1	**0.6**	**1.1**

gridpoint value or the neighborhood maximum value (i.e., STP_{80km}) for the preceding 40-km grid hour, STP increases as tornado damage classifications increase (Fig. 8). Supercell events tended to exhibit higher STP values than QLCS and other modes for the same EF-scale damage rating. The STP for supercell, QLCS, and other modes tended to increase monotonically with increasing damage class ratings (aside from the 10th percentile). Substantial overlap exists in the distributions between adjacent EF-scale ratings, though the higher values of STP_{80km} (i.e., ≥6) are more common for a greater proportion of supercell events at higher EF-scale rating classes (i.e., EF3+). Tornadic supercells by EF scale had higher median STP_{80km} values than QLCS, and tornadic QLCSs had higher STP_{80km} values than other modes. Statistically significant differences in STP_{80km} values (Table 2) were found between EF4+, EF3, and EF2 supercell classes using a two-sample tailed difference of means Student's *t* test, which complements findings by Brotzge et al. (2013) from a similar, independent dataset.

It must be stressed that composite parameters such as the STP_{80km} should not be examined alone, but rather in concert with the individual components in the STP that identify important supercell tornado ingredients. Despite the promise of STP_{80km} as a relatively simple environmental diagnostic to assess the potential for tornadoes, there is no replacement for a thorough diagnosis of the spatiotemporal distribution of buoyancy, shear, and moisture. Furthermore, anticipating changes to the near-storm environment via airmass modification near boundaries, storm interactions, etc., provides an observational foundation for the effective use of SPC mesoanalysis data.

d. Relationship among environment, 0.5° peak V_{rot}, and EF-scale rating

As shown in T12, the differences in effective storm-relative helicity (ESRH; Thompson et al. 2007) between weak and strong tornado environments are larger than the differences in MLCAPE. The mean values of ESRH increase more rapidly than the mean

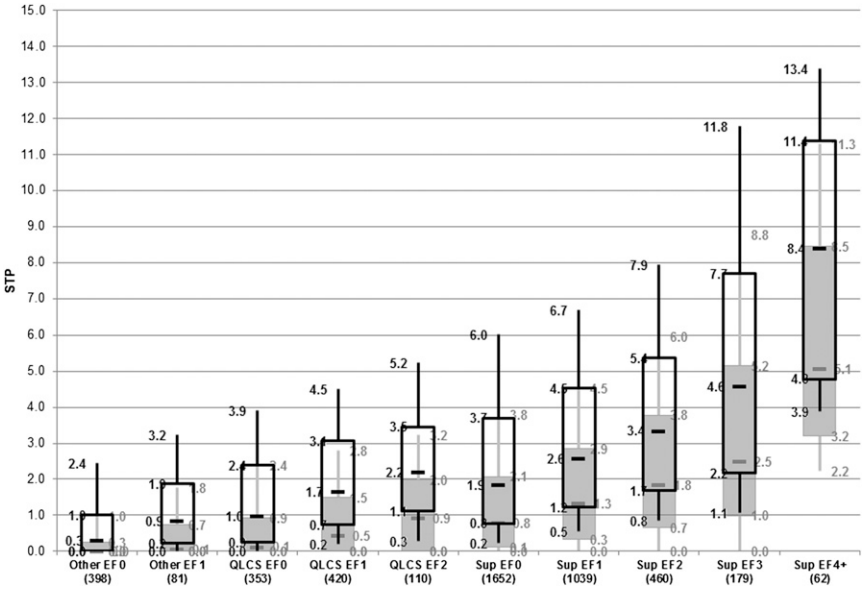

FIG. 8. Box-and-whiskers plot of effective-layer STP (dimensionless) for all supercell, QLCS EF0–EF2, and other modes EF0 and EF1 by EF-scale damage rating classes (40-km grid data are shaded gray, labels on right). Black overlays (labels on left) denote STP_{80km} values, at the analysis time immediately preceding the event time. Other conventions are the same as in Fig. 3.

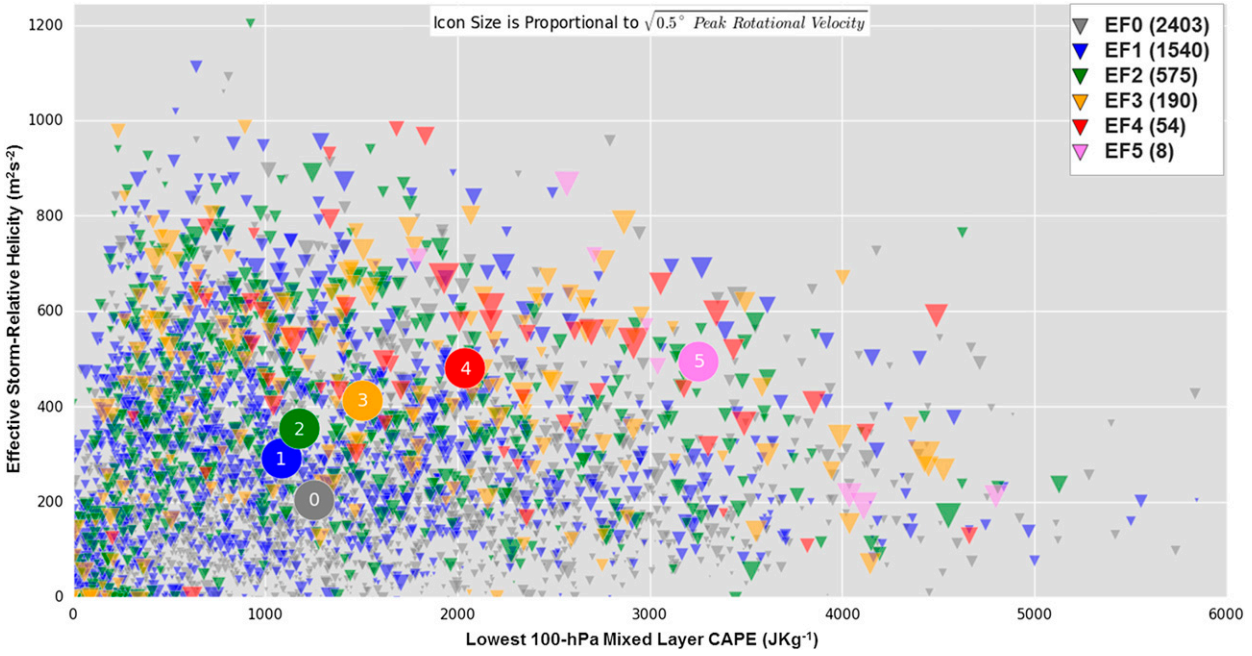

FIG. 9. Scatterplot of EF0–EF5 tornado events (2009–13; inverted triangle symbol) by EF-scale rating (legend at top right) of 100-hPa mixed layer CAPE (J kg^{-1}; x coordinate) vs effective storm-relative helicity (m^2 s^{-2}; y coordinate) and 0.5° peak V_{rot} proportionately sized to velocity strength. The circles represent the mean values of ESRH and MLCAPE for each EF-scale rating.

values of MLCAPE at the lower EF-scale tornado damage ratings (i.e., from EF0 to EF2; Fig. 9). However, MLCAPE exhibits an increasing influence on mean EF-scale tornado damage ratings transitioning from the middle to upper EF scale (i.e., from EF2 to EF5).

Weakly damaging tornado events primarily occupy the distribution space featuring weaker velocities and low STP_{80km} values (Fig. 10). Strong tornadoes (i.e., EF2 and EF3) tend to mostly occur with $V_{rot} \geq 40$ kt but across much of the STP_{80km} parameter space (e.g., 0.5–15). Violent tornadoes (EF4+) were found to generally

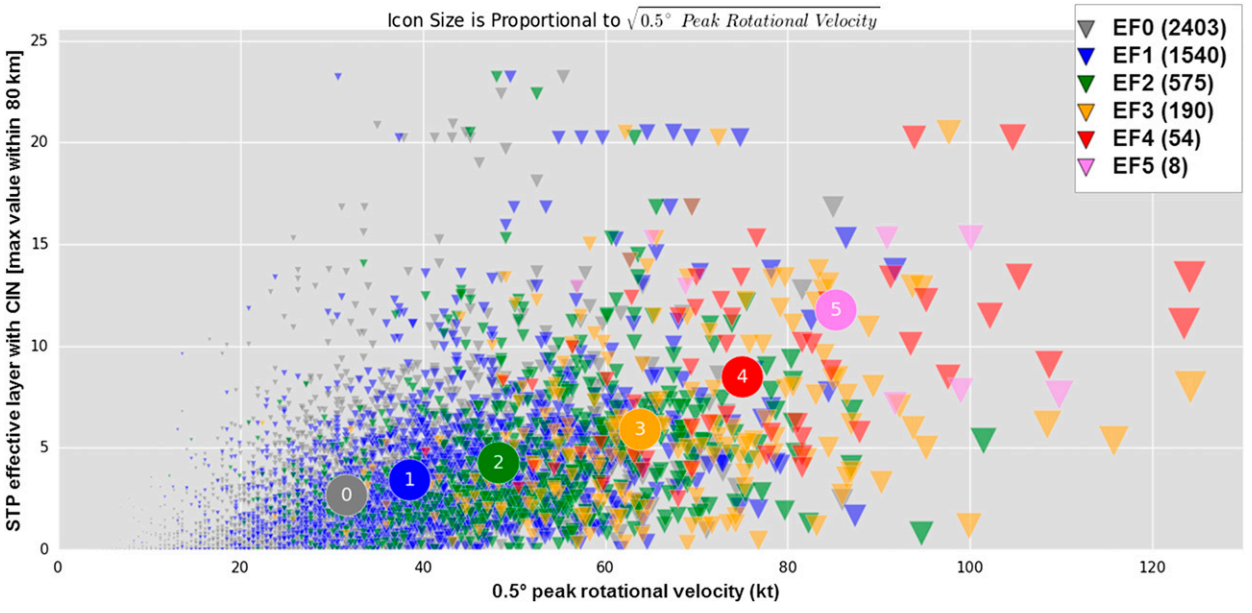

FIG. 10. As in Fig. 9, but for 0.5° peak V_{rot} (kt) vs STP_{80km} (dimensionless).

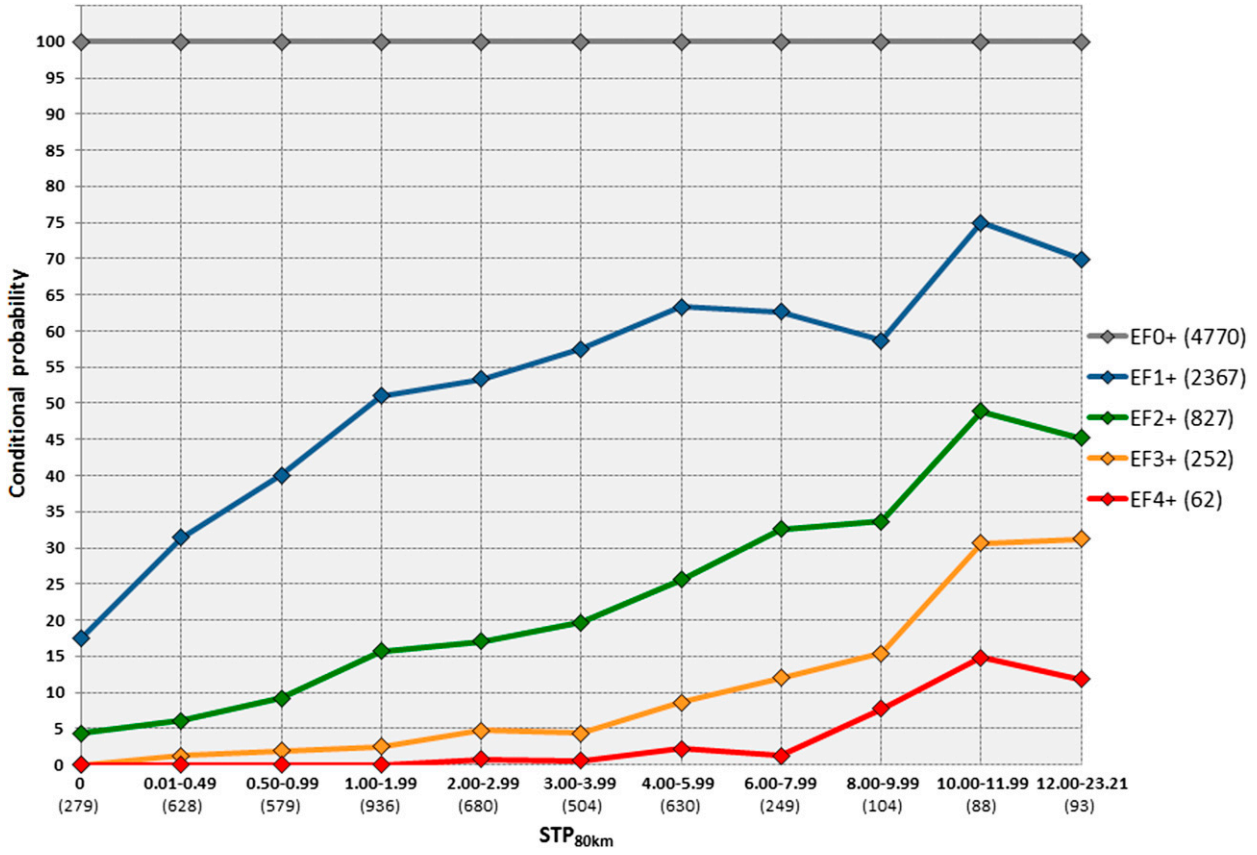

FIG. 11. Conditional probability of meeting or exceeding a given EF-scale rating (legend) for STP_{80km} (dimensionless; *x* coordinate; sample size) for all convective mode tornado events (2009–13; at ≤10 000 ft ARL, with 1–101-mi radius).

favor both extreme 0.5° peak V_{rot} (≥90 kt) and near-storm environments ($STP_{80km} \geq 8$). Mean EF-scale tornado damage ratings increase owing to both strengthening 0.5° peak V_{rot} and higher values of STP_{80km} (Fig. 10).

The direct relationship between 0.5° peak V_{rot} and tornado damage ratings (i.e., stronger V_{rot} associated with higher ratings) can be extended to other attributes of tornadoes. For example, Brooks (2004) suggests that stronger tornadoes are associated with both 1) wider damage paths and 2) longer pathlengths. Furthermore, tornado intensity is a fundamental component of the destruction potential index (DPI; Thompson and Vescio 1998; Doswell et al. 2006), which is a parameter that characterizes tornado impact. As a logical extension of these relationships, very strong 0.5° peak V_{rot} signatures (conditional upon a tornado; >80 kt) imply the possibility of more intense, wider, and longer-track tornadoes that can impact larger areas and potentially exert a greater societal impact in the form of damage and fatalities. We find that these larger, more intense, and longer-lived tornadic circulations are better resolved by the WSR-88D and are sampled by a greater number of radar volume scans per tornado life cycle compared to small, weak, and short-track (short lived) tornadoes.

e. Conditional probabilities of tornado intensity

Another potentially valuable way to extract meaningful real-time information involves examining the relationship among STP_{80km}, 0.5° peak V_{rot}, and EF-scale damage via conditional exceedance probabilities of EF-scale damage ratings (i.e., given a tornado, what is the probability of damage of at least a certain rating?). The relatively large sample size of tornado EF-scale ratings enables this study to examine differences and similarities across EF-scale ratings. The conditional probability of tornado damage intensity exhibits a strong, yet seemingly robust and stable, signal of increasing probability for higher EF scale as both STP_{80km} and 0.5° peak V_{rot} increase (Figs. 11 and 12). An overwhelming majority (i.e., ≥90%) of tornado events within environments <1 STP_{80km} or <30 kt for 0.5° peak V_{rot} are weak tornadoes (EF0

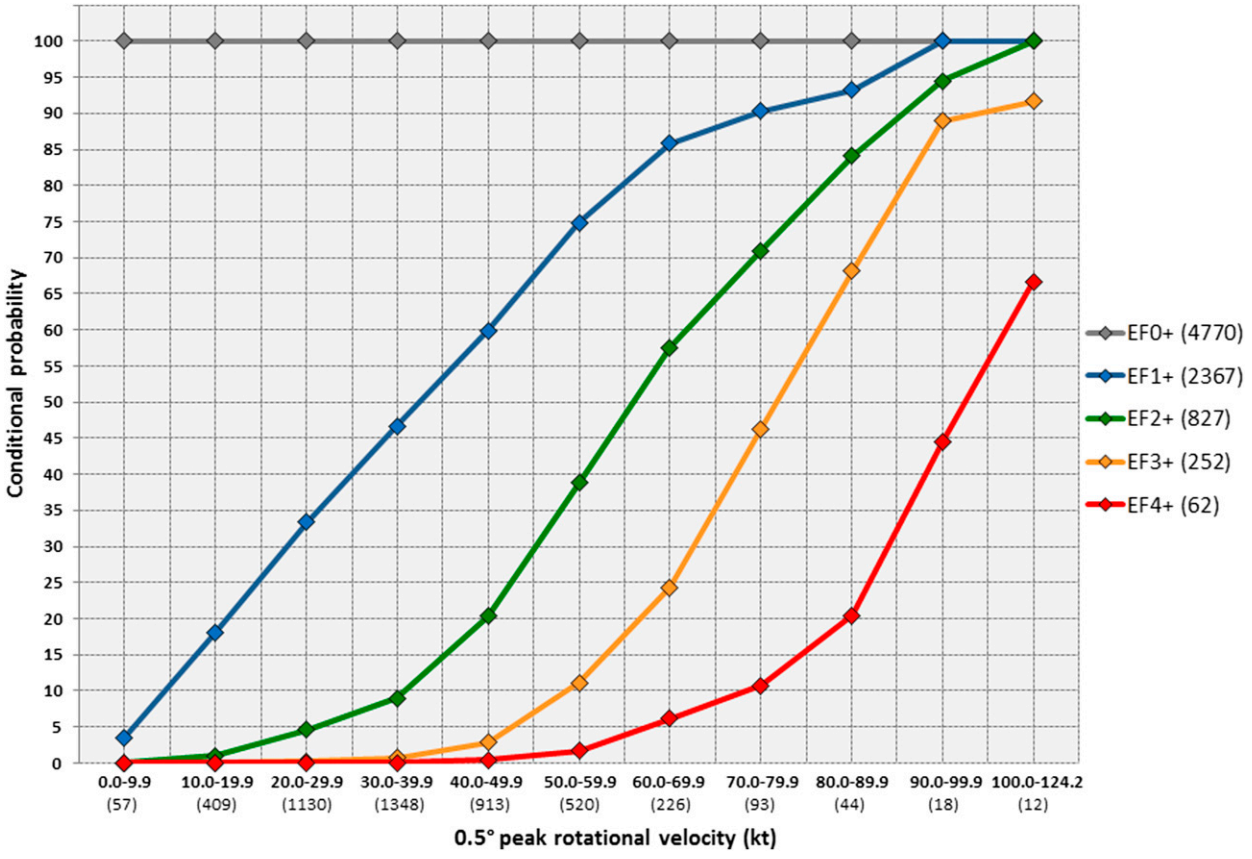

FIG. 12. As in Fig. 11, but for 0.5° peak V_{rot} (kt; x coordinate).

and EF1). This is illustrated in Figs. 11 and 12, where the probability of EF2+ events is less than or equal to 10% at the aforementioned STP_{80km} and 0.5° peak V_{rot} thresholds and below. As the environment becomes more favorable for tornadic supercells and STP_{80km} rises from the lower single digits to 10 or higher, the conditional probabilities for an EF2+ increase from 15%–20% to 45%–50% (Fig. 11). A similar overall trend is displayed in Fig. 12 as 0.5° peak V_{rot} increases, but a larger increase in conditional probabilities is evident with higher EF scale compared to STP_{80km}. Conditional probabilities based solely on 0.5° peak V_{rot} for EF2+ events are 55%–60% when 0.5° peak V_{rot} ranges from 60.0 to 69.9 kt. Even though the sample size of the tornado events with 0.5° peak V_{rot} of 80 kt or higher is small, the proportion of very damaging tornadoes increases markedly (i.e., rapid increase in conditional probabilities). For example, 0.5° peak V_{rot} ranging from 80.0 to 89.9 kt results in conditional probabilities of 65%–70% for EF3+ events and 20% for EF4+ events. To achieve high confidence (i.e., >75%) in damage ratings of EF1+ or EF3+, 0.5° peak V_{rot} must meet or exceed the 50–59.9-and 90–99.9-kt ranges, respectively. Grouping EF-scale tornado events into weak (EF0 and EF1), strong (EF2 and EF3), and violent (EF4 and EF5) categories (Fig. 13) offers a simple way to amplify differences in the distribution of conditional probabilities. The conditional probability of a weak tornado is larger than the other EF-scale categories at weaker V_{rot} (i.e.,<60 kt), whereas strong and violent tornado event categories have probability maxima displaced at stronger 0.5° peak V_{rot} magnitudes (80.0–89.9 and 100.0–124.2 kt, respectively).

Both STP_{80km} and 0.5° peak V_{rot} information were binned and plotted together (Fig. 14) to provide the conditional probability of an EF2+ tornado, similar to a forecaster having both datasets to consider in real time. Conditional EF2+ tornado probabilities increase by ~50% as 0.5° peak V_{rot} increases from 40 to 80 kt for all STP_{80km} values. A smaller increase (~15%) in conditional EF2+ tornado probabilities is evident as STP_{80km} increases from 0 to 10 within a range of 40–80-kt 0.5° peak V_{rot}. Combining both pieces of information yields the largest increase in

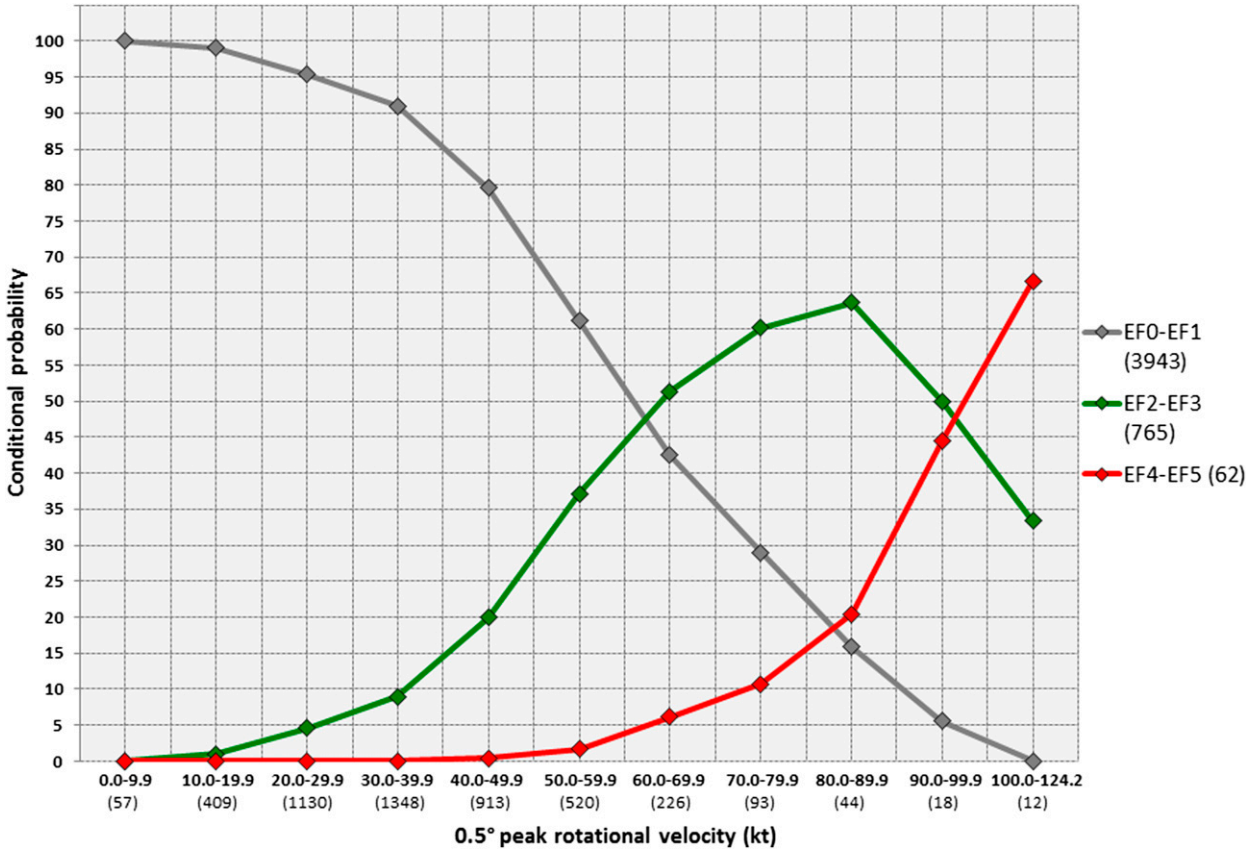

FIG. 13. Conditional probability of grouped EF-scale rating classes (legend on right; EF0 and EF1, EF2 and EF3, and EF4 and EF5) for 0.5° peak V_{rot} (kt; x coordinate; sample size) for all convective mode tornado events (2009–13; at ≤10 000 ft ARL, with 1–101-mi radius).

conditional EF2+ probabilities. Specifically, an increase from 40-kt 0.5° peak V_{rot} with near-zero STP_{80km} to 80-kt 0.5° peak V_{rot} in an environment with STP_{80km} around 10 results in a more than 65% increase in conditional EF2+ tornado probability, effectively demonstrating the utility of combining both datasets to best discriminate between EF0 and EF1 and EF2–EF5 tornado events.

4. Summary and discussion

Over 4700 tornado events during 2009–13 were analyzed from a spatially diverse sampling of tornadic storm modes and environments within 101 mi of operational WSR-88D radars. As part of a comprehensive convective mode–environment investigation at the SPC, both previous foundational studies (i.e., S12 and T12) highlighted the relationship between convective mode, mesocyclone strength, and tornado damage ratings. Additionally, T12 combined near-storm environment data (e.g., STP) with a large sample of tornado events and validated that high STP, right-moving supercell convective mode, and strong mesocyclones yielded the greatest risk for EF3+ tornadoes. However, T12 found substantial overlap in STP distributions by EF-scale rating (T12, their Fig. 12) and emphasized the following statement: ''confident delineation in damage categories will prove difficult for individual storms during a particular hour based on storm mode and environment alone.'' Their assertion served as the primary motivation to develop a dataset with greater precision of the parent tornadic storm low-level circulation intensity than was done previously in S12 (i.e., 1-kt V_{rot} increments vs three broad categories of mesocyclone strength). The additional work was completed by manually assigning 0.5° peak V_{rot} to tornado events, and this highlighted a distinct relationship between tornado event characteristics (i.e., radar attributes) and tornado damage ratings.

This study demonstrates the usefulness of a multiple-dataset approach to better assess the conditional probability of maximum tornado EF scale by combining information on the near-storm environment, convective mode, and 0.5° peak V_{rot} (Fig. 15). This approach can be applied operationally by considering the following:

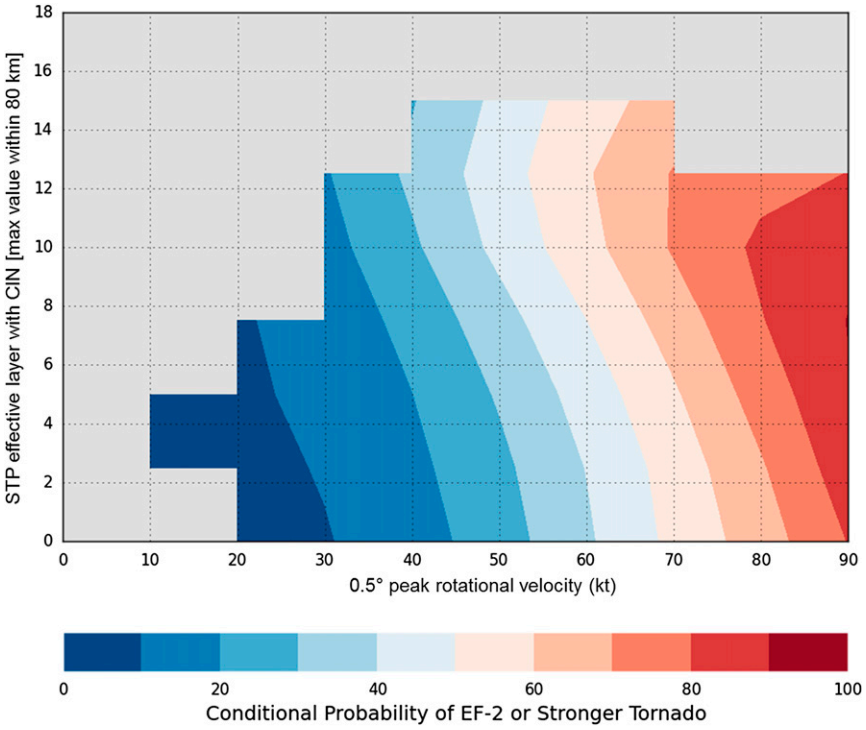

FIG. 14. Smoothed conditional probability of EF2+ tornado rating (shaded) of 0.5° peak V_{rot} (kt; x coordinate) vs STP_{80km} (dimensionless; y coordinate). The conditional probability is only calculated and shown for bins with at least one EF2+ tornado.

1) real-time comparison of available observations with the model-based estimates of the storm environment, 2) real-time monitoring of storm structure and rotational characteristics via WSR-88D sampling, and 3) supporting evidence of a tornado via the development of a dual-polarization tornadic debris signature (DPTDS; e.g., Bodine et al. 2013; Schultz et al. 2012a,b; Bunkers and Baxter 2011) with vertical and temporal continuity, since a majority of tornadoes are not reported to local National Weather Service offices in real time (Blair and Leighton 2014). When observations corroborate the model-based estimates, and velocity signatures show spatial, temporal, and vertical continuity in the storm's low levels, confidence can be higher in the application of the conditional probabilities derived from 0.5° peak V_{rot}. Conversely, disagreement between observations and model-based estimates of the environment, or sharp gradients among the meteorological variables with few corresponding observations, would suggest lower confidence in an expected outcome. Undoubtedly, a continued critical evaluation by operational forecasters (Guyer and Hart 2012) is needed to provide a case-by-case diagnosis and short-term prediction of the atmosphere while considering the inherent assumptions and limitations of this simplified situational awareness approach. While the conditional probability approach is not intended explicitly for tornado warnings with lead time, the STP_{80km} and 0.5° peak V_{rot} can aid in anticipating decision thresholds as the warning decision-making process evolves. Specifically, making use of 0.5° peak V_{rot} trends and corresponding changes in conditional tornado strength probabilities during tornado warnings can be used by the warning forecaster to both assess changes in intensity and confidence to convey tornado intensification in severe weather statements accompanying tornado warnings on an event-driven basis.

False alarms are probable with strict application of the technique (e.g., Fig. 15) when there is no confirming evidence of a tornado. A case from the evening of 31 August 2014 illustrates the potential for false alarms. A supercell in Fremont County, Iowa, exhibiting a 0.5° peak V_{rot} of 63 kt at 0102 UTC and an estimated STP_{80km} value near 7 in the 0000 UTC SPC mesoanalysis data (not shown), resulted in a ~53% conditional EF2+ probability. However, the strongest V_{rot} with the storm was confined to only a 5-min period (the 0059–0104 UTC scans), and there was no corresponding DPTDS. Additionally, though the SPC mesoanalysis data from 0100 UTC admittedly would not have been available

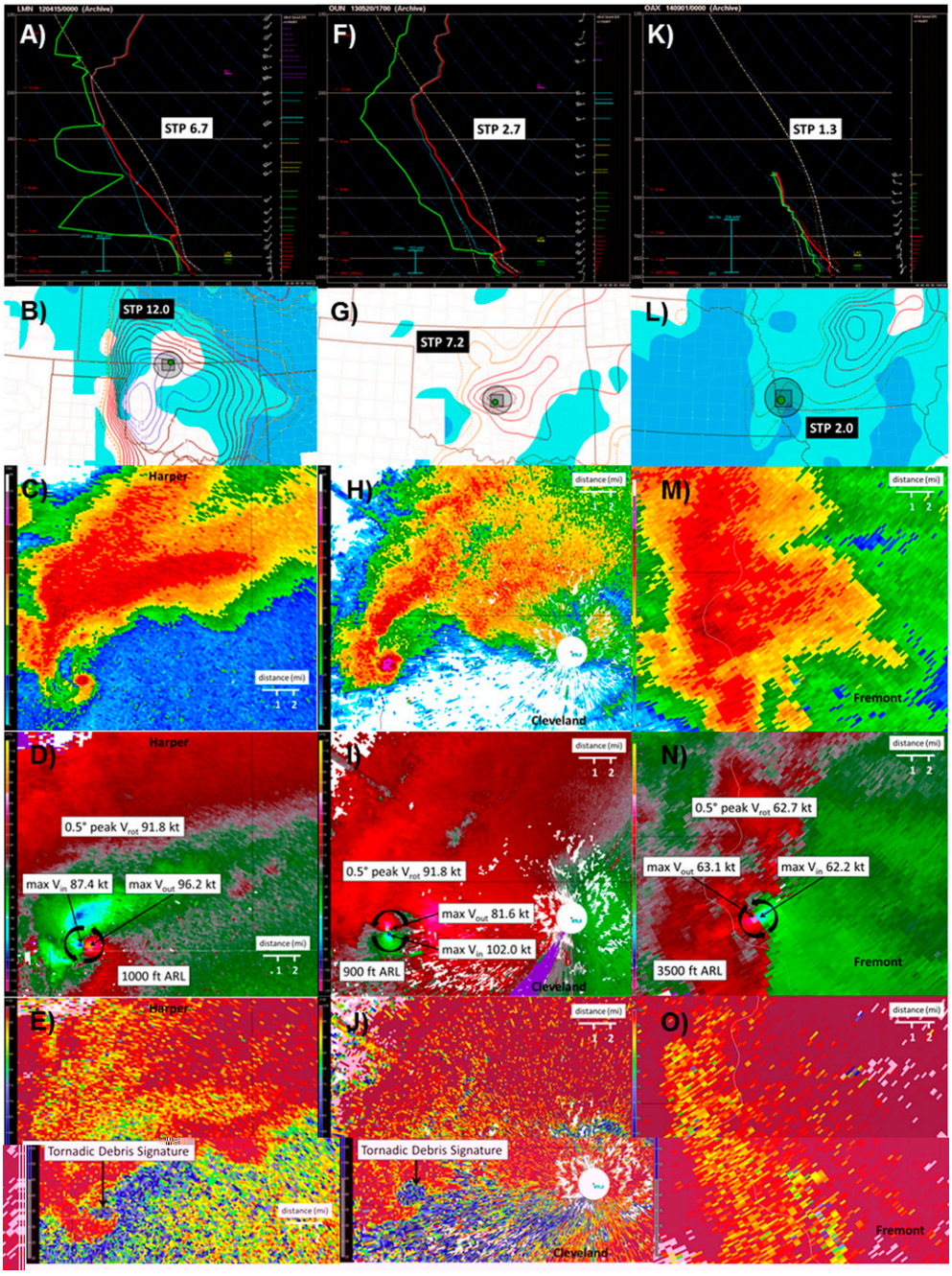

FIG. 15. (a) Observed sounding from Lamont, OK, at 0000 UTC 15 Apr 2012, with STP 6.7. (b) Harper County, KS, tornadic storm location (green circle), SPC mesoanalysis 40-km grid (black square), and 80-km radius (black circle), with STP_{80km} 12.0. (c) As in Fig. 1a, but for Vance Air Force Base, OK (KVNX), at 0142 UTC 15 Apr 2012. A discrete-cell supercell produced an EF1 tornado event in Harper County, KS. (d) As in Fig. 1b, but for KVNX for max V_{in} (87.4 kt), max V_{out} (96.2 kt), and 0.5° peak V_{rot} (91.8 kt) sampled at 1000 ft ARL. (e) KVNX WSR-88D dual-pol cross-correlation coefficient (ρ_{hv}) indicative of a tornadic debris signature. (f) As in (a), but for Norman, OK, at 1700 UTC 20 May 2013, with STP 2.7. (g) As in (b), but for Cleveland County, OK. Note that the smoothed planar STP value (5–6) is different than STP_{80km} 7.2. (h) As in (c), but for Twin Lakes, OK (KTLX), at 2012 UTC 20 May 2013. A discrete-cell supercell produced an EF5 tornado event in Cleveland County, OK. (i) As in (d), but for KTLX for max V_{in} (102.0 kt), max V_{out} (81.6 kt), and 0.5° peak V_{rot} (91.8 kt), sampled at 900 ft ARL. (j) As in (e), but for KTLX. (k) As in (a), but for Omaha, NE, at 0000 UTC 1 Sep 2014, with STP 1.3. As in (b), but for Fremont County, IA, with STP_{80km} 7.2. (m) As in (c), but for Omaha/Valley, NE (KOAX), at 0102 UTC 1 Sep 2014. A cell-in-cluster supercell was nontornadic and produced a wind damage report in Fremont County, IA. (n) As in (d), but for KOAX for max V_{in} (62.2 kt), max V_{out} (63.1 kt), and 0.5° peak V_{rot} (62.7 kt) sampled at 3500 ft ARL. (o) As in (e), but for KOAX with no evidence of a tornadic debris signature.

TABLE A1. Archived SPC mesoanalysis variables. Parameters are nondimensional where no units are listed, and abbreviations are as follows: lowest 100-hPa mean layer (ML), surface based (SB), most unstable lowest 300 hPa (MU), and maximum 50-hPa mean layer (best).

STP_{80km} (fixed layer)	STP (fixed layer)
STP_{80km} (effective layer with CIN)	STP (effective layer with CIN)
Effective inflow base	STP (Thompson et al. 2003)
SCP_{80km} (effective layer)	SCP (effective layer)
ML, SB, MU, best CAPE ($J\,kg^{-1}$)	0–8, 0–6, 0–3, 0–1-km effective bulk wind difference (kt)
ML, SB, MU, best CIN ($J\,kg^{-1}$)	0–3, 0–1 effective storm-relative helicity ($m^2\,s^{-2}$)
ML, MU, LCL (m AGL)	0–3-km, 850–500-hPa, 700–500-hPa lapse rate ($°C\,km^{-1}$)
ML, MU, LFC (m AGL)	Surface temp (°F)
Downdraft CAPE ($J\,kg^{-1}$)	Surface dewpoint temp (°F)
0–3-km CAPE (Jkg^{-1})	Surface relative humidity (%)
Significant hail parameter	Precipitable water (in.)

until ~0125 UTC, a substantial decrease in STP_{80km} from ~7 to ~2 was noted from 0000 to 0100 UTC. The lack of a real-time tornado report in this example, combined with the lack of a DPTDS and a decrease in STP_{80km} over time, suggested that an EF2+ was unlikely. Work is ongoing to develop a large null sample to create unconditional tornado probabilities to aid in the real-time diagnosis of tornado potential.

Acknowledgments. This study benefited from early discussions with Dr. Israel Jirak and Steven Weiss (SPC), Dr. Harold Brooks (NSSL), and James LaDue (WDTB), as well as a manuscript review by Dr. Jirak. We thank three anonymous reviewers for valuable suggestions and constructive criticisms that prompted us to better clarify our thoughts in this manuscript.

APPENDIX

SPC Mesoanalysis Variables

Table A1 provides information on archived SPC mesoanalysis variables.

REFERENCES

Alexander, C. R., and J. M. Wurman, 2008: Updated mobile radar climatology of supercell tornado structures and dynamics. Preprints, *24th Conf. Severe Local Storms,* Savannah, GA, Amer. Meteor. Soc., 19.4. [Available online at https://ams.confex.com/ams/pdfpapers/141821.pdf.]

Andra, D. L., Jr., 1997: The origin and evolution of the WSR-88D mesocyclone recognition nomogram. Preprints, *28th Conf. on Radar Meteorology,* Austin, TX, Amer. Meteor. Soc., 364–365.

Benjamin, S. G., and Coauthors, 2004: An hourly assimilation–forecast cycle: The RUC. *Mon. Wea. Rev.,* **132,** 495–518, doi:10.1175/1520-0493(2004)132<0495:AHACTR>2.0.CO;2.

Blair, S. F., and J. W. Leighton, 2014: Assessing real-time tornado information disseminated through NWS products. *Wea. Forecasting,* **29,** 591–600, doi:10.1175/WAF-D-13-00126.1.

Bodine, D. J., M. R. Kumjian, R. D. Palmer, P. L. Heinselman, and A. V. Ryzhkov, 2013: Tornado damage estimation using polarimetric radar. *Wea. Forecasting,* **28,** 139–158, doi:10.1175/WAF-D-11-00158.1.

Bothwell, P. D., J. A. Hart, and R. L. Thompson, 2002: An integrated three-dimensional objective analysis scheme in use at the Storm Prediction Center. Preprints, *21st Conf. on Severe Local Storms,* San Antonio, TX, Amer. Meteor. Soc., J117–J120. [Available online at https://ams.confex.com/ams/pdfpapers/47482.pdf.]

Brady, R. H., and E. J. Szoke, 1989: A case study of nonmesocyclone tornado development in northeast Colorado: Similarities to waterspout formation. *Mon. Wea. Rev.,* **117,** 843–856, doi:10.1175/1520-0493(1989)117<0843:ACSONT>2.0.CO;2.

Brooks, H. E., 2004: On the relationship of tornado path length and width to intensity. *Wea. Forecasting,* **19,** 310–319, doi:10.1175/1520-0434(2004)019<0310:OTROTP>2.0.CO;2.

Brotzge, J. A., S. E. Nelson, R. L. Thompson, and B. T. Smith, 2013: Tornado probability of detection and lead time as a function of convective mode and environmental parameters. *Wea. Forecasting,* **28,** 1261–1275, doi:10.1175/WAF-D-12-00119.1.

Bunkers, M. J., and M. A. Baxter, 2011: Radar tornadic debris signatures on 27 April 2011. *Electron. J. Oper. Meteor.,* **12** (7). [Available online at http://www.nwas.org/ej/2011/2011.php.]

Burgess, D. W., R. L. Lee, S. S. Parker, S. J. Keighton, and D. L. Floyd, 1995: A study of mini supercells observed by WSR-88D radars. Preprints, *27th Conf. on Radar Meteorology,* Vail, CO, Amer. Meteor. Soc., 4–6.

Coniglio, M. C., 2012: Verification of RUC 0–1-km forecasts and SPC mesoscale analyses using VORTEX2 soundings. *Wea. Forecasting,* **27,** 667–683, doi:10.1175/WAF-D-11-00096.1.

Craven, J. P., and H. E. Brooks, 2004: Baseline climatology of sounding derived parameters associated with deep, moist convection. *Natl. Wea. Dig.,* **28,** 13–24.

Crum, T. D., R. L. Alberty, and D. W. Burgess, 1993: Recording, archiving, and using WSR-88D data. *Bull. Amer. Meteor. Soc.,* **74,** 645–653, doi:10.1175/1520-0477(1993)074<0645:RAAUWD>2.0.CO;2.

Davies, J. M., 1993: Small tornadic supercells in the central plains. Preprints, *17th Conf. Severe Local Storms,* St. Louis, MO, Amer. Meteor. Soc., 305–309.

——, 2004: Estimations of CIN and LFC associated with tornadic and nontornadic supercells. *Wea. Forecasting,* **19,** 714–726, doi:10.1175/1520-0434(2004)019<0714:EOCALA>2.0.CO;2.

——, and A. Fischer, 2009: Environmental characteristics associated with nighttime tornadoes. *Electron. J. Oper. Meteor.,*

10 (3). [Available online at http://www.nwas.org/ej/2009/2009.php].

Davis, J. M., and M. D. Parker, 2014: Radar climatology of tornadic and nontornadic vortices in high-shear, low-CAPE environments in the Mid-Atlantic and southeastern United States. *Wea. Forecasting,* **29,** 828–853, doi:10.1175/WAF-D-13-00127.1.

Doswell, C. A., III, R. Edwards, R. L. Thompson, J. A. Hart, and K. C. Crosbie, 2006: A simple and flexible method for ranking severe weather events. *Wea. Forecasting,* **21,** 939–951, doi:10.1175/WAF959.1.

Eilts, M. D., and S. D. Smith, 1990: Efficient dealiasing of Doppler velocities using local environment constraints. *J. Atmos. Oceanic Technol.,* **7,** 118–128, doi:10.1175/1520-0426(1990)007<0118:EDODVU>2.0.CO;2.

French, M. M., H. B. Bluestein, I. PopStefanija, C. A. Baldi, and R. T. Bluth, 2013: Reexamining the vertical development of tornadic vortex signatures in supercells. *Mon. Wea. Rev.,* **141,** 4576–4601, doi:10.1175/MWR-D-12-00315.1.

Grant, B. N., and R. Prentice, 1996: Mesocyclone characteristics of mini supercell thunderstorms. Preprints, *15th Conf. on Weather Analysis and Forecasting,* Norfolk, VA, Amer. Meteor. Soc., 362–365.

Guyer, J. L., and J. A. Hart, 2012: Examination of WSR-88D VWP data in proximity to strong tornadoes. Preprints, *26th Conf. on Severe Local Storms,* Nashville, TN, Amer. Meteor. Soc., 62. [Available online at https://ams.confex.com/ams/26SLS/webprogram/Paper211652.html.]

Kennedy, P. C., N. E. Westcott, and R. W. Scott, 1993: Single-Doppler radar observations of a mini-supercell tornadic thunderstorm. *Mon. Wea. Rev.,* **121,** 1860–1870, doi:10.1175/1520-0493(1993)121<1860:SDROOA>2.0.CO;2.

Kingfield, D. M., J. G. LaDue, and K. L. Ortega, 2012: An evaluation of tornado intensity using velocity and strength attributes from the WSR-88D mesocyclone detection algorithm. Preprints, *26th Conf. on Severe Local Storms,* Nashville, TN, Amer. Meteor. Soc., 3.2. [Available online at https://ams.confex.com/ams/26SLS/webprogram/Paper211488.html.]

LaDue, J. G., K. L. Ortega, B. R. Smith, G. J. Stumpf, and D. M. Kingfield, 2012: A comparison of high resolution tornado surveys to Doppler radar observed mesocyclone parameters: 2011–2012 case studies. Preprints, *26th Conf. on Severe Local Storms,* Nashville, TN, Amer. Meteor. Soc., 6.3. [Available online at https://ams.confex.com/ams/26SLS/webprogram/Paper212627.html.]

Laflin, J. M., 2013: Verification of RAP model soundings in pre-convective environments. *J. Oper. Meteor.,* **1** (6), 66–70, doi:10.15191/nwajom.2013.0106.

Magsig, M. A., 2008: New techniques for integrating environmental information with radar base data analysis in National Weather Service warning decision making. Preprints, *24th Conf. on Severe Local Storms,* Savannah, GA, Amer. Meteor. Soc., P6.10. [Available online at https://ams.confex.com/ams/24SLS/techprogram/paper_142264.htm.]

Mitchell, E. D., S. V. Vasiloff, G. J. Stumpf, A. Witt, M. D. Eilts, J. T. Johnson, and K. W. Thomas, 1998: The National Severe Storms Laboratory tornado detection algorithm. *Wea. Forecasting,* **13,** 352–366, doi:10.1175/1520-0434(1998)013<0352:TNSSLT>2.0.CO;2.

Newman, J. F., V. Lakshmanan, P. L. Heinselman, M. B. Richman, and T. M. Smith, 2013: Range-correcting azimuthal shear in Doppler radar data. *Wea. Forecasting,* **28,** 194–211, doi:10.1175/WAF-D-11-00154.1.

Parker, M. D., 2014: Composite VORTEX2 supercell environments from near-storm soundings. *Mon. Wea. Rev.,* **142,** 508–529, doi:10.1175/MWR-D-13-00167.1.

Potvin, C. K., K. L. Elmore, and S. J. Weiss, 2010: Assessing the impacts of proximity sounding criteria on the climatology of significant tornado environments. *Wea. Forecasting,* **25,** 921–930, doi:10.1175/2010WAF2222368.1.

Rasmussen, E. N., 2003: Refined supercell and tornado forecast parameters. *Wea. Forecasting,* **18,** 530–535, doi:10.1175/1520-0434(2003)18<530:RSATFP>2.0.CO;2.

——, and D. O. Blanchard, 1998: A baseline climatology of sounding-derived supercell and tornado forecast parameters. *Wea. Forecasting,* **13,** 1148–1164, doi:10.1175/1520-0434(1998)013<1148:ABCOSD>2.0.CO;2.

ROC, 2014: NEXRAD coverage below 10,000 feet AGL. NOAA/Radar Operations Center, accessed 1 September 2014. [Available online at http://www.roc.noaa.gov/WSR88D/Maps.aspx.]

Schultz, C. J., and Coauthors, 2012a: Dual-polarization tornadic debris signatures Part I: Examples and utility in an operational setting. *Electron. J. Oper. Meteor.,* **13** (9), 120–137. [Available online at http://www.nwas.org/ej/2012/2012.php.]

——, and Coauthors, 2012b: Dual-polarization tornadic debris signatures Part II: Comparisons and caveats. *Electron. J. Oper. Meteor.,* **13** (10), 138–150. [Available online at http://www.nwas.org/ej/2012/2012.php.]

Smith, B. T., R. L. Thompson, J. S. Grams, C. Broyles, and H. E. Brooks, 2012: Convective modes for significant severe thunderstorms in the contiguous United States. Part I: Storm classification and climatology. *Wea. Forecasting,* **27,** 1114–1135, doi:10.1175/WAF-D-11-00115.1.

Smith, T. M., and K. L. Elmore, 2004: The use of radial velocity derivatives to diagnose rotation and divergence. Preprints, *11th Conf. on Aviation, Range, and Aerospace,* Hyannis, MA, Amer. Meteor. Soc., P5.6. [Available online at http://ams.confex.com/ams/pdfpapers/81827.pdf.]

Speheger, D. A., and R. D. Smith, 2006: On the imprecision of radar signature locations and storm path forecasts. *Natl. Wea. Dig.,* **30,** 3–10.

Stensrud, D. J., J. V. Cortinas Jr., and H. E. Brooks, 1997: Discriminating between tornadic and nontornadic thunderstorms using mesoscale model output. *Wea. Forecasting,* **12,** 613–632, doi:10.1175/1520-0434(1997)012<0613:DBTANT>2.0.CO;2.

——, and Coauthors, 2009: Convective-scale warn-on-forecast system: A vision for 2020. *Bull. Amer. Meteor. Soc.,* **90,** 1487–1499, doi:10.1175/2009BAMS2795.1.

Stumpf, G. J., A. Witt, E. D. Mitchell, P. L. Spencer, J. T. Johnson, M. D. Eilts, K. W. Thomas, and D. W. Burgess, 1998: The National Severe Storms Laboratory mesocyclone detection algorithm for the WSR-88D. *Wea. Forecasting,* **13,** 304–326, doi:10.1175/1520-0434(1998)013<0304:TNSSLM>2.0.CO;2.

Thompson, R. L., and M. D. Vescio, 1998: The destruction potential index: A method for comparing tornado days. Preprints, *19th Conf. Severe Local Storms,* Minneapolis, MN, Amer. Meteor. Soc., 280–282.

——, R. Edwards, J. A. Hart, K. L. Elmore, and P. M. Markowski, 2003: Close proximity soundings within supercell environments obtained from the Rapid Update Cycle. *Wea. Forecasting,* **18,** 1243–1261, doi:10.1175/1520-0434(2003)018<1243:CPSWSE>2.0.CO;2.

——, C. M. Mead, and R. Edwards, 2007: Effective storm-relative helicity and bulk shear in supercell thunderstorm environments. *Wea. Forecasting,* **22,** 102–115, doi:10.1175/WAF969.1.

——, B. T. Smith, J. S. Grams, A. R. Dean, and C. Broyles, 2012: Convective modes for significant severe thunderstorms in the contiguous United States. Part II: Supercell and QLCS tornado environments. *Wea. Forecasting,* **27,** 1136–1154, doi:10.1175/WAF-D-11-00116.1.

——, ——, A. R. Dean, and P. T. Marsh, 2013: Spatial distributions of tornadic near-storm environments by convective mode. *Electron. J. Severe Storms Meteor.,* **8** (5). [Available online at http://www.ejssm.org/ojs/index.php/ejssm/issue/view/47.]

Torres, S. M., and C. D. Curtis, 2007: Initial implementation of super-resolution data on the NEXRAD network. Preprints, *23rd Int. Conf. on Interactive Information Processing Systems,* San Antonio, TX, Amer. Meteor. Soc., 5B.10. [Available online at http://ams.confex.com/ams/pdfpapers/116240.pdf.]

Toth, M., R. J. Trapp, J. Wurman, and K. A. Kosiba, 2013: Comparison of mobile-radar measurements of tornado intensity with corresponding WSR-88D measurements. *Wea. Forecasting,* **28,** 418–426, doi:10.1175/WAF-D-12-00019.1.

Trapp, R. J., and M. L. Weisman, 2003: Low-level mesovortices within squall lines and bow echoes. Part II: Their genesis and implications. *Mon. Wea. Rev.,* **131,** 2804–2823, doi:10.1175/1520-0493(2003)131<2804:LMWSLA>2.0.CO;2.

——, S. A. Tessendorf, E. S. Godfrey, and H. E. Brooks, 2005: Tornadoes from squall lines and bow echoes. Part I: Climatological distribution. *Wea. Forecasting,* **20,** 23–34, doi:10.1175/WAF-835.1.

Wagenmaker, R., G. Mann, and M. Hudson, 2014: IBW project: Introduction and overview. NOAA/NWS, accessed 15 July 2014. [Available online at http://www.crh.noaa.gov/images/dtx/GLOMW/Presentations/2014_IBW_Project_Intro_Overview.pdf.]

Wilks, D. S., 2006: *Statistical Methods in the Atmospheric Sciences.* 2nd ed. International Geophysics Series, Vol. 59, Academic Press, 627 pp.

Wood, V. T., and R. A. Brown, 1997: Effects of radar sampling on single-Doppler velocity signatures of mesocyclones and tornadoes. *Wea. Forecasting,* **12,** 928–938, doi:10.1175/1520-0434(1997)012<0928:EORSOS>2.0.CO;2.

Zittel, W. D., and Z. Jing, 2012: Comparison of a 2-D velocity dealiasing algorithm to the legacy WSR-88D velocity dealiasing algorithm during Hurricane Irene. Preprints, *30th Conf. on Hurricanes and Tropical Meteorology,* Ponte Vedra Beach, FL, Amer. Meteor. Soc., 7C.7. [Available online at https://ams.confex.com/ams/30Hurricane/webprogram/Paper205076.html.]